HoxD cluster scanning deletions identify multiple defects leading to paralysis in the mouse mutant *Ironside*

Basile Tarchini,[1] Thi Hanh Nguyen Huynh,[1] Greg A. Cox,[2] and Denis Duboule[1,3]

[1]National Research Centre 'Frontiers in Genetics' and Department of Zoology and Animal Biology, University of Geneva, 1211 Geneva 4, Switzerland; [2]The Jackson Laboratory, Bar Harbor, Maine 04609, USA

A spontaneous semidominant mutation (*Ironside, Irn*) was isolated in mice, leading to severe hindlimb paralysis following multiple deletions in *cis* at the *HoxD* locus. To understand its cellular and molecular etiology, we embarked on a comparative analysis using systematic *HoxD* cluster deletions, produced via targeted meiotic recombination (TAMERE). Different lines of mice were classified according to the severity of their paralyses, and subsequent analyses revealed that multiple causative factors were involved, alone or in combination, in the occurrence of this pathology. Among them are the loss of *Hoxd10* function, the sum of remaining *Hoxd* gene activity, and the ectopic gain of function of the neighboring gene *Evx2*, all contributing to the mispositioning, the absence, or misidentification of specific lumbo-sacral pools of motoneurons, nerve root homeosis, and hindlimb innervation defects. These results highlight the importance of a systematic approach when studying such clustered gene families, and give insights into the function and regulation of *Hox* and *Evx2* genes during early spinal cord development.

[*Keywords*: Homeosis; peroneal nerve; chromosome engineering; motoneuron]

Supplemental material is available at http://www.genesdev.org.

Received May 11, 2005; revised version accepted October 3, 2005.

Mammalian genomes contain 39 *Hox* genes, organized in four clusters; *HoxA* to *HoxD* (McGinnis and Krumlauf 1992). These series of contiguous genes encode transcription factors necessary for proper development to proceed. Coordinate expression of *Hox* genes, in both time and space, is partly dictated by their order along the chromosome, such that genes are activated one after the other, from the 3′-end of the gene cluster toward its 5′-extremity. Genes activated early on will establish an anterior expression boundary in a variety of trunk derivatives, whereas subsequent activations will generate progressively more posterior boundaries, following molecular mechanisms that only begin to be understood (Kmita and Duboule 2003).

Collinear *Hox* gene expression is found in many developing systems, such as in paraxial mesoderm (Gaunt et al. 1988), in the digestive and the uro-genital tracts (Dollé et al. 1991; Yokouchi et al. 1995), or in budding limbs (Dollé et al. 1991). It is also observed in the embryonic spinal cord and hindbrain, where *Hox* genes are characterized by a precise rostral expression boundary (Gaunt et al. 1988). The function of these genes during the development of the central nervous system (CNS) has been addressed in the presumptive rhombencephalon, due to the existence of morphological and molecular landmarks. The importance of *Hox* gene products in both the segmental organization of hindbrain neurons (Lumsden and Krumlauf 1996) and neural crest derivatives (Trainor and Krumlauf 2001) was thus demonstrated.

Yet few studies have addressed the function of *Hox* genes in the spinal cord, due to both the difficulty of assigning morphological landmarks and the functional redundancy of the *Hox* system (Carpenter 2002). Consequently, while *Hox* gene loss-of-function approaches lead to alterations in vertebral morphologies, neural alterations at comparable body levels are more difficult to document, in particular outside the limb territories, which seem to require more complex *Hox*-associated patterning information such as that necessary to organize finer topological distinctions. Accordingly, roles for these genes in the spinal cord have been mostly linked to the brachial and lumbo-sacral plexii, innervating the fore- and hindlimbs, respectively. For example, mice lacking *Hoxc8* function display an aberrant forelimb connectivity pattern (Tiret et al. 1998), and *Hoxd10* disruption resulted in hindlimb gait and position defects

[3]**Corresponding author.**
E-MAIL Denis.Duboule@zoo.unige.ch; FAX 41-22-379-6795.
Article and publication are at http://www.genesdev.org/cgi/doi/10.1101/gad.351105.

associated with reduction in both the peroneal nerve and the terminal arborization of the tibial nerve, suggesting that alterations in motoneuron (MN) positional identities impacted on the peripheral innervation pattern (Carpenter et al. 1997; Wahba et al. 2001).

Hox gene expression in the spinal cord is dynamic, often starting in broad ventricular regions, before postmitotic neural commitment occurs, and subsequently maintained in some MN or interneuron (IN) subtypes. Interestingly, paralogous genes from different clusters have related AP expression domains but may respond to distinct dorsoventral patterning signals (Graham et al. 1991; Davenne et al. 1999). Recently, a functional relationship between *Hox* expression and MN specification was documented as HOXC6 and HOXC9 protein expression coincided with particular brachial and thoracic motoneurons (Dasen et al. 2003). Ectopic expression of either protein induced both the extinction of the other and a concomitant change in MN subtype. Therefore, HOX cross-repressive interactions may establish distinct rostro-caudal MN fate as well as MN pool identity within a given columnar subtype (Dasen et al. 2003). Likewise, *Hoxd10* could specify the lateral motor column (LMC) at lumbar levels (Shah et al. 2004).

A mouse with a severe semidominant hindlimb paralysis was discovered, which carried a spontaneous mutation allelic to the *HoxD* cluster. To understand why this phenotype was more severe than that induced by a targeted deletion of the entire cluster (Zakany et al. 2001) and gain insights into the role of *Hox* genes in hindlimb motricity, we engineered a set of targeted deletions (TAMERE) (Hérault et al. 1998). The analysis of various deleted strains and the new mutant stock allowed us to distinguish between different categories of phenotypes and to correlate these categories with distinct defects in MN specification and axonal projection at lumbo-sacral levels. This systematic approach shed light on the function of *Hox* genes in the specification of MN and identified the ectopic expression of *Evx2* as the cause of the most severe phenotype, in addition to the loss of *Hoxd10* function.

Results

The Ironside *mutation is allelic to* HoxD

A mouse with a spontaneous mutation was isolated due to severe hindlimb paralysis (Fig. 1A). Further crosses narrowed down the mutated locus to a 6-cM interval between D2Mit10 and D2Mit418 on chromosome 2. Heterozygous mice were bred to homozygosity, which produced an even more severe condition with complete hindlimb paralysis as well as digit malformations. Recessive digit shortening suggested that *Hoxd* genes, located within the interval, were involved (Dollé et al. 1993), and subsequent PCR amplification indicated that mutant mice had lost *Hoxd13* to *Hoxd8*, whereas the neighboring *Evx2* and *Hoxd4* genes were intact.

The cloning of the breakpoints revealed a double deletion in *cis*, separated by a short piece of DNA. The first deletion removed a 43-kb large fragment containing from *Hoxd13* to *Hoxd9*, whereas the second contained an 8-kb large fragment including the second exon of *Hoxd8* and 3′ sequences (Fig. 1B). The two deletions were separated by the first exon of *Hoxd8* and part of its 5′-UTR and intronic sequences, linked to a 200-base-pair (bp) fragment coming from an inverted duplication of a noncoding locus located 394 kb centromeric to the *Evx2* gene.

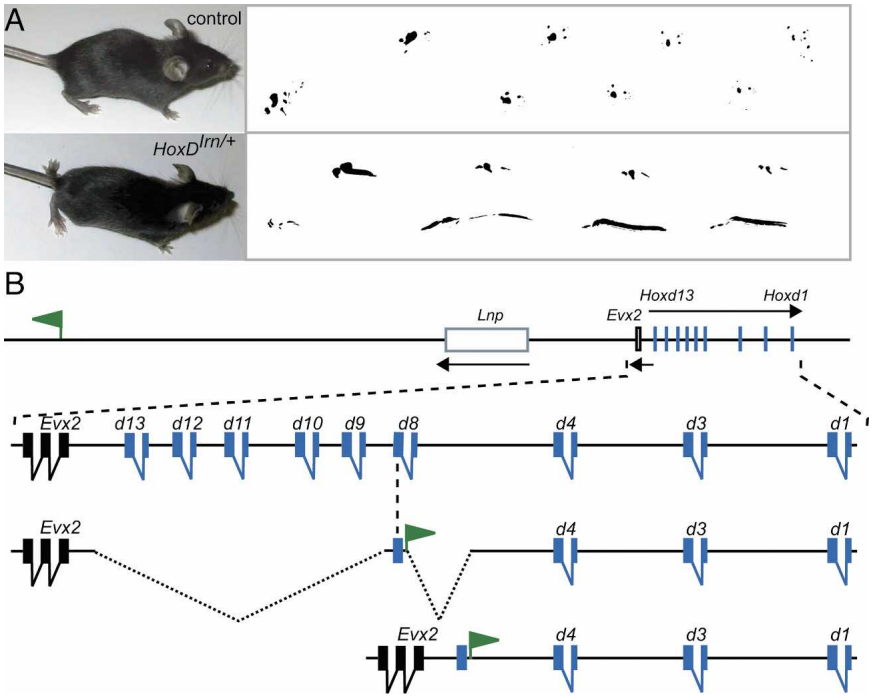

Figure 1. The spontaneous mutation *Ironside* (*Irn*). (*A*, *bottom*) Mice heterozygous for *Irn* (*HoxD*$^{Irn/+}$) display severe hindlimb paralysis, as illustrated by footprint analyses. (*B*) The *Irn* mutation is a combined deletion/insertion event at the *HoxD* cluster. *Hox* genes are indicated in blue, whereas *Evx2* is in black. The mutated locus contains two deletions in *cis* (dashed lines) removing from *Hoxd13* to within *Hoxd8*, and from within *Hoxd8* further 3′. A fragment of *Hoxd8* was left in place (*bottom* line; blue box), along with a piece of DNA translocated from a region located centromeric to the locus (*top* and *bottom* lines; green flag). This latter, noncoding sequence is still present at its original locus in the mutant configuration, in an inverted orientation. No other genomic rearrangement was detected outside the *HoxD* cluster.

This latter locus appeared nevertheless intact in mutant mice. This mutant stock, called *Ironside* (*Irn*), is therefore an allele of the *HoxD* cluster [Del(*2Hoxd8,Hoxd9-Hoxd13*)], referred to below as $HoxD^{Irn}$ or *Irn*.

TAMERE-induced deletions reveal classes of paralyzed phenotypes

To understand the molecular etiology of this severe phenotype, we produced four mouse strains carrying a *LoxP* site targeted between selected pairs of *Hoxd* genes (Fig. 2, L5, L6, L7, L8). These mice, as well as others previously available (Fig. 2, L1, L4, L11), were intercrossed to induce unequal meiotic recombinations, leading to the deleted strains depicted in Figure 2. We selected a set of deletions resembling the *Irn* mutation, that is, starting upstream of *Hoxd13*. We also analyzed smaller internal deletions, with or without *Hoxd10*, as loss of function of this gene induced mild hindlimb defects (Carpenter et al. 1997). These deletion stocks are referred to as, for example, Del(10–13), for the $HoxD^{Del(10–13)}$ allele (a deletion removing from *Hoxd10* to *Hoxd13*). One deletion was associated with the *cis* inactivation of the neighboring gene *Evx2* [Del(10–13); $Evx2^{stop}$]. The intergenic region between *Hoxd4* and *Hoxd8*, flanked by the L7 and L8 *loxP* sites, was named region "i."

This collection of mutant animals revealed a range of defects in locomotion and posture. Complete hindlimb paralysis was scored in specimens homozygous for three different deletions, all with a 5′ breakpoint between *Evx2* and *Hoxd13* [Fig. 2, Del(10–13), Del(9–13), and Del(i–13)]. The defects were similar to those in the *Irn* mutant, confirming that the *HoxD* rearrangement was the cause of the *Irn* paralysis. These three deletions and

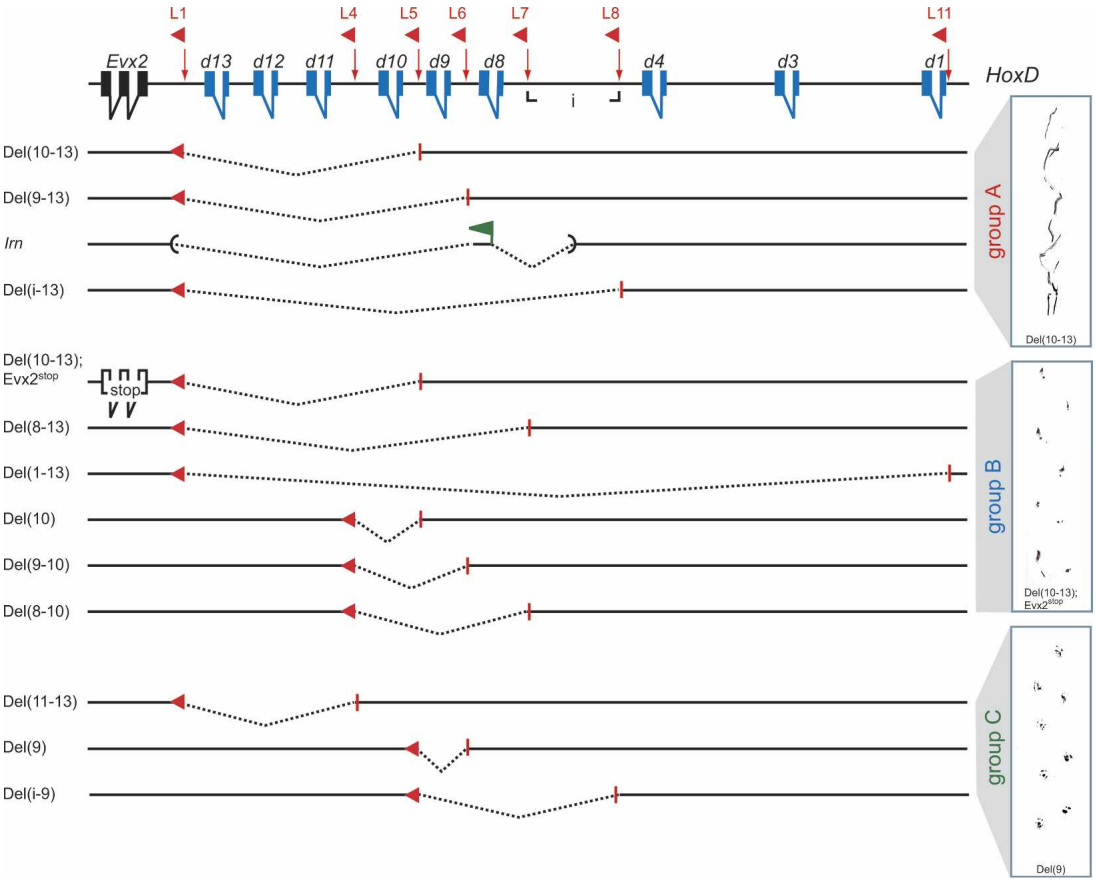

Figure 2. Scheme of deleted mouse strains used in this work. On the *top*, the *HoxD* cluster with the position of the various *LoxP* sites (red). Each site represents an independent mouse strain. The strains containing the L5, L6, L7, and L8 sites were produced for this study, whereas others were described previously. *Below* are 11 deleted strains generated by recombinations between pairs of *LoxP* parental lines using the technique TAMERE (Hérault et al. 1998). The *Ironside* (*Irn*) and Del(1–13) alleles are also included. Breakpoints are in red, with a triangle for the remaining *LoxP* site. The deleted fragments are shown in dashed lines. For convenience, the strains are referred to as, for example, Del(10–13) for a deletion removing from *Hoxd10* to *Hoxd13*, inclusively [$HoxD^{Del(10–13)}$]. One configuration carries in addition a stop codon engineered within the neighboring *Evx2* gene ($Evx2^{stop}$). These deleted strains are classified in three groups, with the same color code throughout the paper, based on the severity of the paralysis, documented by footprint analyses of representative homozygous specimen. Group A (red) deletions are dominant and lead to complete paralysis, whereas group B (blue) animals have a recessive and less severe phenotype. Group C (green) animals have no obvious hindleg problem. The inactivation of *Evx2* in the Del(10–13) deletion significantly rescues the locomotion defect.

the *Irn* allele also shared a semidominant phenotype and were referred to as "group A" alleles (Fig. 2).

A second set of deletions (Fig. 2, Group B) showed more heterogeneous phenotypes, less severe than in group A, with recessive locomotion defects due to a distally restricted leg paralysis, even though they shared with group A their 5′ breakpoint [Fig. 2, Del(10–13); *Evx2*^{stop} and Del(8–13)]. Animals of this group could bear their body weight on the hindlegs and retained left–right alternation in walking (Fig. 2, cf. footprints). Foot placement and gait were reminiscent of clubfoot phenotypes (e.g., Helmbacher et al. 2000). Interestingly, the full *HoxD* deficiency (Zakany et al. 2001) fell into this group, as well as internal deletions lacking the *Hoxd10* gene [Fig. 2, Del(10), Del(9–10), and Del(8–10)]. Finally, a third class of strains (Fig. 2, group C) displayed apparently normal locomotion and posture. These included one stock with a breakpoint at the L1 position [Fig. 2, Del(11–13)], as well as internal deletions [Fig. 2, Del(9), Del(i–9)], all of them leaving *Hoxd10* intact.

Peroneal nerve defects in HoxD *deletions*

These deleted strains showed no detectable alteration in embryonic limb muscle patterning. Instead, striking defects were observed in the peroneal nerve branch of mutant fetuses. This branch emanates from the dorso-sacral hindlimb plexus and targets various muscles, among which are the extensors of the leg latero-distal compartment. Anti-neurofilament immunostaining revealed a range of peroneal defects, already visible at day 12.5. Peroneal nerve branches were classified as "close to normal," "thinner and/or shorter," "truncated," or "absent" (Fig. 3A). In the former category, the growth of peroneal branches was comparable to that of the adjacent tibial branch. While thinner and/or shorter peroneal branches entered the limb bud, they contained fewer fibers and/or showed reduced or delayed distal progression. Truncated branches displayed a nerve trunk past the plexus region, but few fibers had entered the limb bud proper at embryonic day 13.5 (E13.5). The "absent" category referred to a

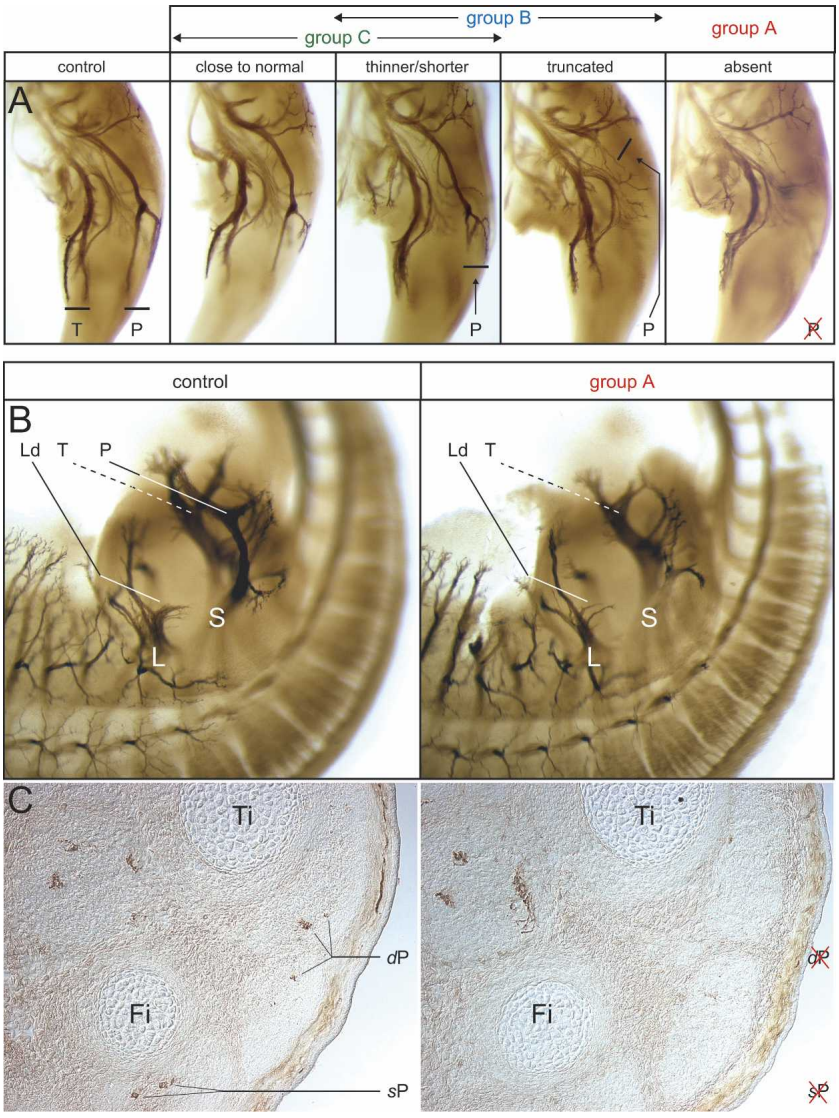

Figure 3. Peroneal nerve defects in *HoxD* deletion strains. (*A*) Whole-mount neurofilament immunostainings of E12.5–E13.5 hindlimbs (posterior view, dorsal is right and distal at the bottom) differentiate various peroneal nerves as "close to normal," "thinner/shorter," and "truncated" or "absent." Group C animals show close to normal or thinner/shorter peroneal nerves; group B animals display thinner/shorter or truncated phenotype, whereas severely affected group A animals show no peroneal nerve. (*B*, *right*) In addition to the complete loss of the dorso-sacral plexus and emanating peroneal nerve (P), group A mutants also show innervation defects in the dorso-lumbar plexus (Ld), where fewer fibers are visible. Pictures are lateral views of a right hindlimb. (*C*) E14.5 leg cross-sections at shank level stained for neurofilaments revealed the absence of the deep (dP) and superficial (sP) peroneal nerves in group A specimens. (T) Tibial nerve (ventral); (P) peroneal nerve (dorsal); (L) lumbar plexus (anterior); (S) sacral plexus (posterior); (Fi) fibula; (Ti) tibia.

very thin peroneal nerve, likely consisting of sensory components only.

While group C animals showed close to normal or thinner/shorter peroneal branches (Fig. 3A), group B alleles led to variable proportions of thinner/shorter versus truncated branches. Expectedly, peroneal branches were absent in group A animals (Fig. 3A,B), and cross-sections of E14.5 hindlimbs at shank level confirmed the loss of the peroneal nerves (Fig. 3C). Dissection of adult legs revealed the absence of the common peroneal nerve with full or partial penetrance in group A and B animals, respectively. Furthermore, a severe atrophy of the leg antero-lateral compartment muscles was observed in group A animals, suggesting subsequent degeneration. This tight correlation with the severity of the paralysis indicated that peroneal innervation defects play a major role in the phenotype. Neurofilament staining of group A embryos also revealed other peripheral nerve defects such as a reduced dorso-lumbar plexus (Fig. 3B). The tibial branch, originating from the ventro-sacral plexus, appeared normal in all deleted stocks (Fig. 3A,B).

Nerve roots homeosis

As innervation deficits can arise from alterations in either peripheral navigation, or the neuronal specification in the spinal cord, we looked at lumbo-sacral (LS) spinal root morphology in the various deletions and scored several defects. LS spinal roots have distinct migratory trajectories, which confer their unique identities. In wild-type embryos, the 21st–23rd roots contribute to the lumbar plexus, whereas the 23rd–25th contribute to the sacral (sciatic) plexus (Fig. 5A, below). For each plexus, axonal fibers adopt either a ventral or a dorsal trajectory after entering the limb bud.

Homeotic transformations were observed in several deleted alleles. They were mostly recessive and changed a nerve root into the identity of its rostral neighbor, such that the LS root pattern appeared shifted posteriorly (anterior homeosis). Transformations were often partial and some LS nerve roots could be transformed, whereas others remained unchanged. For example, in the Del(10–13); $Evx2^{stop}$ allele, only the 25th and 26th roots appeared transformed into the 24th and 25th identities, respectively (Fig. 4C). Incomplete transformations with a mixed roots profile are illustrated by the *Irn* mutant, where, in addition to a full transformation of the 25th and 26th roots, the 23rd and 24th roots appeared only partially transformed into 22nd and 23rd root identities, respectively (Fig. 4B). In contrast, Del(10) mutant mice displayed a complete and dominant posterior transformation, with all LS roots transformed into the identity of the next caudal neighbor (Fig. 4D). Consequently, the LS nerve pattern was normal yet displaced rostrally, leading to the loss of one thoracic root.

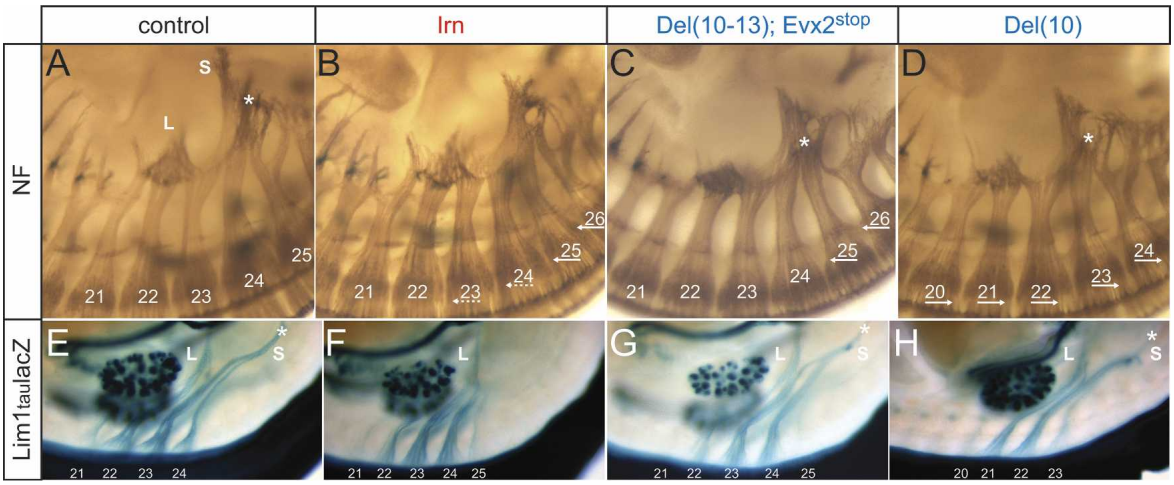

Figure 4. Homeotic transformations in *HoxD* deletion strains. (*A*) Neurofilament stainings at E11.5–E12.5 show that roots 21–23 participate in the lumbar plexus, whereas roots 23–25 form the sacral plexus, with characteristic projection patterns. (*B*) The 21st and 22nd roots are unchanged in *Irn* mutants, whereas more caudal roots are transformed into anterior identities, with different magnitudes, such that, for example, the 25th and 26th mutant roots appear like normal 24th and 25th. (*C*) Transformations are more restricted in Del(10–13); $Evx2^{stop}$ mutants, as only the caudal-most 25th and 26th roots appeared transformed. (*D*) In contrast, posterior transformations are seen in the Del(10) allele, with all LS roots looking like their immediate posterior neighbor. (*E*) Crosses between *HoxD* deletions and a *Lim1taulacZ* knock-in transgenic line reveal the motor projections to the dorsal limb. Motor fibers in roots 21–24 are labeled, whereas only few (if any) fibers are detected in the 25th root. (*F*) The *Irn* mutant shows two motor defects: the absence of the dorso-sacral plexus (S) and anterior homeotic transformations. In this latter case, projections from the 23rd root mostly target the lumbar plexus, instead of going to both lumbar and sacral plexii, and the 25th root is stained, indicating a more anterior identity. (*G*) In contrast, a dorso-sacral plexus is visible in Del(10–13); $Evx2^{stop}$ mutants, which have more subtle anterior homeosis, such as some positive fibers in the 25th root. (*H*) The Del(10) allele also shows a dorso-sacral plexus, whereas posterior homeosis transformed all motor nerves contributing to the hindlimb. Roots are numbered, with plain and dashed arrows indicating complete or partial transformation, respectively. Arrows to the *left* and *right* indicate anterior and posterior transformations, respectively. (L) Lumbar plexus; (S) sacral plexus. Asterisks indicate the dorso-sacral plexus and emanating peroneal branch.

To discriminate between axonal guidance and spinal autonomous defects, we crossed selected deletion strains with mice carrying a *tau-lacZ* reporter knocked in the *Lim1* gene (Kania et al. 2000). *Lim1* is expressed in the lateral subset of LMC motoneurons, present only at limb levels. As all *Lim1*-positive MN send axons toward the dorsal limb, we visualized the dorsal motor nerve component in our mutant stocks. Control staining showed that only the 23rd and 24th roots contribute to the dorsosacral plexus (Fig. 4E). As the 25th root axons navigate mostly toward the ventral aspect of the sacral plexus, staining was not scored at this level.

Irn embryos showed anterior transformations from the 21st to the 25th motor roots (Fig. 4F). *Lim1*-positive MN included an ectopic caudal population abnormally projecting through the 25th root. These abnormal projections were reduced in the Del(10–13); $Evx2^{stop}$ allele, which showed a weaker homeotic phenotype in the 21st–24th roots region (Fig. 4G). The Del(10) allele displayed global posterior motor nerve homeosis, as with neurofilament staining (Fig. 4H). These results indicated that the homeosis derives from misspecification in the LS spinal cord, the anterior nerve homeosis reflecting a caudal shift in the *Lim1*-positive LMC. Prefiguring limb innervation deficits, group A specimens did not form the dorso-sacral plexus, from which the peroneal branch emerges, whereas group B alleles showed a starting peroneal branch (Fig. 4F,H). In this latter case, fibers must initially converge to the dorso-sacral plexus and initiate a peroneal branch, but further degenerate around the limb entry point. The inability to form a plexus thus correlates with strong motor homeosis in the LS region, as if transformed 24th and 25th roots were unable to endorse a normal 23rd and 24th roots motor profile.

The progressive sequence of anterior homeotic transformations, as induced by the various deletions, is depicted in Figure 5. Homeosis is first seen caudally, suggesting a duplicated 24th root (Fig. 5D, control in C). Further transformations affect the 23rd root, which redirects progressively more axons toward the lumbar plexus at the expense of the sacral plexus (Fig. 5E). During this process, the 21st root usually reduces its contribution to the lumbar plexus. At some point, the 23rd nerve exhibits a 22nd-like morphology, whereas the 22nd and 24th nerves seem to retain their normal identities. Therefore, root patterns suggest the duplication of the 22nd and 24th nerves and, consequently, the absence of a 23rd mixed nerve. Complete transformations affect both the 22nd and 24th roots, which thus adopt a 21st and 23rd profile, respectively, as reported for the loss of function of *Hoxa10* (Fig. 5F; Rijli et al. 1995). Misspecification of nerve trajectories was not necessarily coordinated between the ventral and dorsal aspects (data not shown).

In summary, all group A strains, as well as the majority of group B strains with a breakpoint upstream of *Hoxd13*, displayed partial 21st–24th and complete 25th and 26th roots anterior transformations (Fig. 5E). However, only group A showed severe motor homeosis using the *Lim1taulacZ* marker (Fig. 4F). In contrast, no consistent LS nerve misspecification was scored for group B internal deletions [e.g., Del(9–10); Del(8–10)]. Among group C strains, Del(11–13) showed a full transformation, but restricted to the 25th and 26th roots (Fig. 5D), whereas Del(9) displayed partial 21st–24th and full 25th and 26th transformations (Fig. 5E). The Del(i–9) mice showed no homeosis. Since group B paralysis could occur without spinal root transformation and some transformations in group C had no effect on locomotion, we concluded that homeotic transformations are not a decisive factor in the locomotion defects. The specific partial transformation of the 23rd and 24th motor nerves was nevertheless associated with the strong phenotype of group A specimens.

Spinal cord as the source of the phenotype

These results suggested that alterations in LS nerves led to the observed paralysis. To rule out an impact of mutant hindlimb mesoderm on axonal navigation, we engineered a conditional strain carrying *LoxP* sites flanking the *Hoxd13* and *Hoxd4* genes [Fig. 6I, Flox(4–13)] and used the *Prx1-Cre* deleter transgene (Logan et al. 2002) to induce deletion in growing limbs only, without affecting the developing spinal cord. We looked at the effect in combination with the group A allele Del(10–13). Del(10–13) heterozygous animals often display a thinner and shorter peroneal nerve (Fig. 6A,B), which does not preclude a normal leg posture at birth. However, when a deletion of the *Hoxd4* to *Hoxd13* region [Del(4–13)] was added in *trans*, animals had severely truncated peroneal and bilateral clubfoot phenotypes (Fig. 6D). In contrast, when this latter deletion was induced only in developing limbs, by using the conditional allele, animals were mildly affected (Fig. 6C), with a peroneal branch resembling that of Del(10–13) heterozygous animals. We assessed the efficiency of the conditional deletion by looking at *Hoxd10* transcripts in fetal limbs. In Del(10–13) heterozygotes, *Hoxd10* was expressed in both the limbs and the trunk (Fig. 6A,B). While animals carrying both Del(10–13) and Del(4–13) alleles expectedly had no *Hoxd10* signal, specimens carrying one copy of the conditional allele displayed a signal in the trunk, whereas limbs were devoid of *Hoxd10* mRNAs (Fig. 6G). These results confirmed that the defects in the peroneal branch originate from alterations in the spinal cord, rather than in environmental cues necessary for axonal trajectories.

Molecular bases of spinal cord homeosis

Hox gene losses of function lead to anterior homeotic transformations. Furthermore, "posterior" *Hox* gene products are often functionally dominant over more "anterior" products (posterior prevalence) (Duboule and Morata 1994). In the LS region, *Hoxd10* is the most posterior gene expressed between the 21st and 24th levels, until *Hoxd11* starts to be transcribed at level 25. The former is thus expectedly an essential player for the hindlimb LMC region. Consistently, *HoxD* deletions starting upstream of *Hoxd13* and extending up to at least *Hoxd10*

showed anterior nerve root homeosis. However, internal deletions including *Hoxd10* produced unexpected results; while both Del(9–10) and Del(8–10) showed a wild-type LS root organization, Del(10) had a complete posterior transformation and Del(9) displayed an anterior transformation, as for larger deletions where both *Hoxd11* and *Hoxd10* are missing.

To understand the molecular bases of these unexpected transformations, we analyzed the expression of the remaining *Hoxd* genes in all configurations. While *Hoxd10*, *Hoxd9*, *Hoxd8*, *Hoxd4*, and *Hoxd3* are normally expressed at the LS levels, *Hoxd11* is expressed caudal to the 25th level, and the expression limit of *Hoxd12* and *Hoxd13* is more caudal, making these genes irrelevant in this context. In Del(9), transcription of both *Hoxd10* and *Hoxd11* was shifted posteriorly, leading to anterior homeosis (Fig. 7A,B). Conversely, expression of *Hoxd11* in Del(10) was shifted anteriorly (Fig. 7C). In this latter case, the loss of *Hoxd10* in lumbar spinal cord was more than rescued by the gain of function of *Hoxd11*, leading to a posterior transformation. Related anterior shifts of *Hoxd11* were seen in both Del(9–10) and Del(8–10) alleles, without transformation, likely due to the additional losses of function of *Hoxd9* and *Hoxd8* (Fig. 7D).

This correlation between *Hoxd* gene expression and patterns of homeotic transformations could nevertheless not account for all aspects of the paralysis phenotypes, in particular the difference between group A and B strains. As the full *HoxD* cluster deletion showed a mild group B paralysis, the severity of group A phenotypes could not be explained by multiple losses of function, nor by the observed *Hoxd* genes' gains of function. Since these latter deletions share a breakpoint upstream *Hoxd13* (Fig. 2), near the *Evx2* gene, we looked at *Evx2* expression in various deletions.

Evx2 *misexpression in group A mutants*

Due to the presence of specific enhancers (Spitz et al. 2003) and a *HoxD* insulating mechanism (Kmita et al. 2002), *Evx2* is normally expressed in specific interneurons throughout the developing spinal cord, that is, with a pattern distinct from *Hoxd* genes (Dollé et al. 1994; Moran-Rivard et al. 2001). In *Irn* embryos, we observed a dramatic gain of *Evx2* expression along the entire spinal cord, encompassing virtually all cell types, resembling the neighboring gene *Hoxd4* (Fig. 8A). Analysis of the three other group A alleles, Del(10–13), Del(9–13), and Del(i–13), confirmed this gain of expression, yet with some restriction to the ventral LS region (Fig. 8B; data not shown).

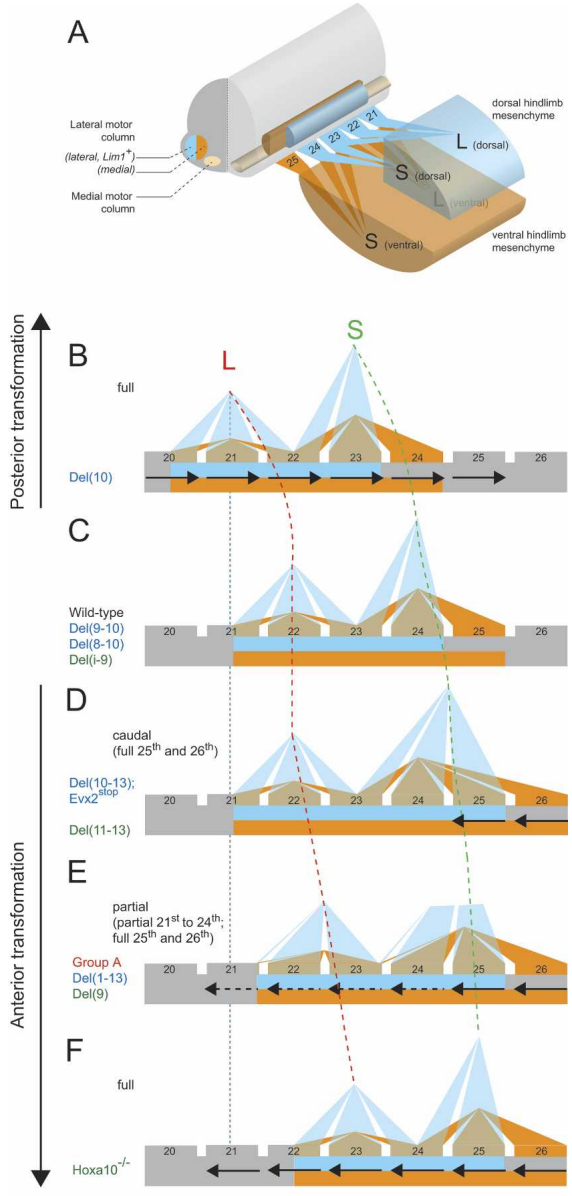

Figure 5. Sequence of progressive homeotic transformations, from a full segment posterior transformation (*B*) to a full segment anterior transformation (*F*). (*A*) Normal hindlimb bud innervation. LMC, nerve roots, plexii, and approximate projections are indicated with a color code used throughout the figure. (*B*) Posterior homeosis observed in Del(10). LS roots are fully transformed toward a posterior projection pattern. (*C*) The wild-type organization is retained in some internal deletions [Del(i–9); Del(8–10); Del(9–10)]. (*D*) Complete anterior transformations, but restricted to the 25th and 26th roots, are scored in group B Del(10–13); $Evx2^{stop}$ and Del(11–13) deletions. In this case, the LMC is caudally extended by one segment such that an additional root contributes to the sacral plexus. (*E*) More severe transformations also affect roots 21–24, to various degrees. The latter roots are nevertheless only partially transformed. For instance, partial transformation of the 23rd root involves rerouting of its axonal projection toward the lumbar plexus, at the expense of the sacral plexus, leading to a root with a hybrid profile between the 22nd and 23rd aspect [group A or Del(1–13) and Del(9) alleles]. (*F*) Full transformation of all lumbar roots following *Hoxa10* inactivation (Rijli et al. 1995), pointing to a full-segment caudal shift of the LMC. Lateral and medial subsets of the LMC are shown in blue and orange, respectively. Arrows to the *right* indicate segment and projection transformation toward a posterior fate, whereas arrows to the *left* indicate the converse transformation.

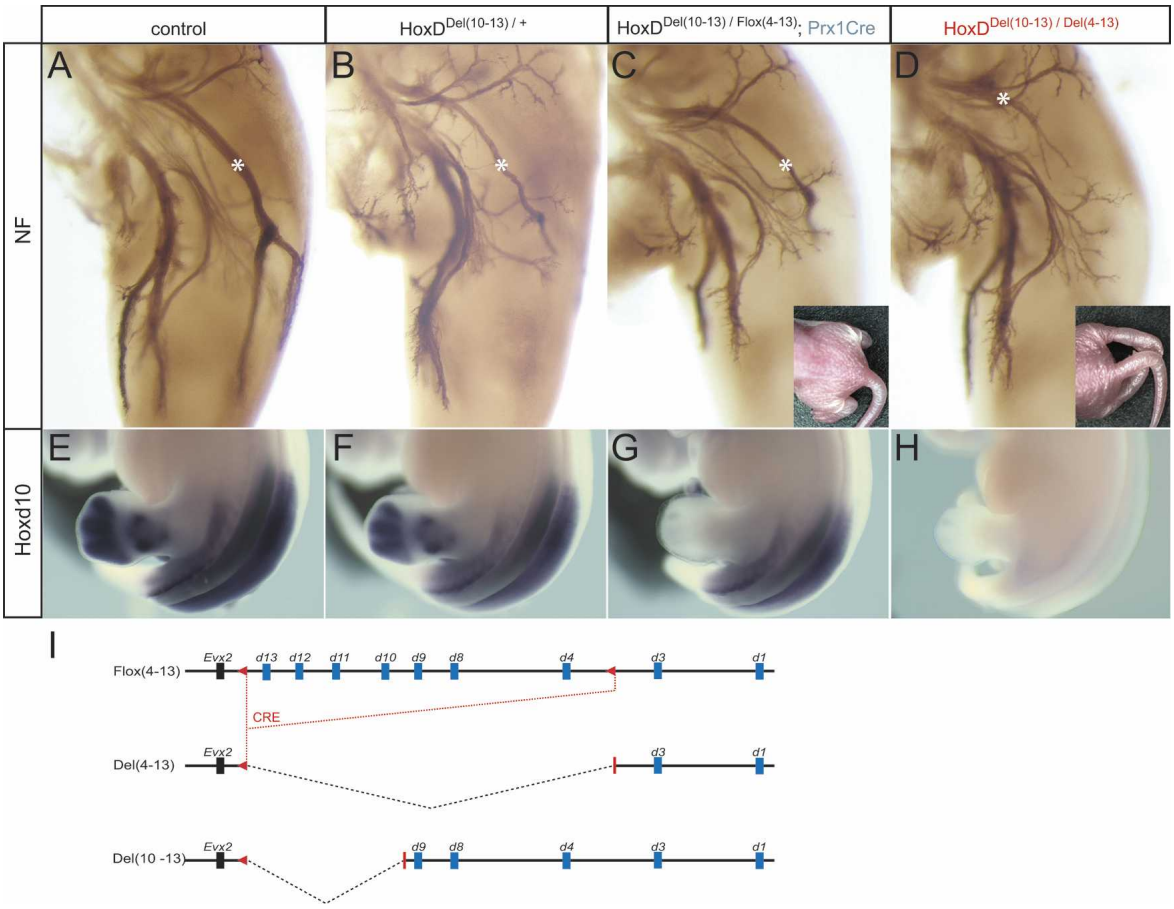

Figure 6. Innervation defects are spinal cord-autonomous. (*A–D*) The floxed *HoxD* allele [Flox(4–13); depicted under *I*] and the *Prx1-Cre* deleter transgene were used to conditionally delete *Hoxd4–Hoxd13* in early developing limb tissues. (*B*, asterisk) Heterozygous Del(10–13) animals often showed a severe peroneal nerve reduction. (*B*,*C*) *Trans*-heterozygous specimens carrying both the Del(10–13) and Flox(4–13) alleles along with the *Prx1-Cre* showed similar peroneal defects, yet with a normal leg posture at birth. (*C*,*D*) In contrast, fully deleted *trans*-heterozygous animals [Del(10–13)/Del(4–13)] showed the expected truncated peroneal nerve and bilateral clubfoot at birth. (*G*) The conditional deletion was monitored by the selective loss of *Hoxd10* expression in E12.5 hindlimb buds.

In contrast, group B alleles sharing the same 5′ breakpoint [Del(8–13) or Del(1–13)] displayed a normal *Evx2* pattern in the spinal cord, as did group C Del(11–13) (Fig. 8B; data not shown). The impact of *Evx2* on the severity of the phenotype was confirmed by the comparison between the Del(10–13) and Del(10–13); $Evx2^{stop}$ alleles. Although these two alleles have the same deletion and a gain of *Evx2* transcripts in the LS spinal cord, only the former belongs to group A, whereas the latter is in group B, demonstrating that a functional EVX2 protein was required for a severe paralysis to occur.

We further engineered a transgenic strain carrying a BAC clone covering the *HoxD* cluster and containing both an *Irn*-like targeted deletion and a *lacZ* cassette in frame within *Evx2* (Fig. 8C). Transgenic mice consistently reproduced the ectopic activation of *Evx2* in the developing spinal cord (Fig. 8D). Furthermore, two distinct lines showed staining in the tibial and peroneal nerve branches emanating from the sacral plexus (Fig. 8D), indicating that the *Evx2* spinal gain of expression had indeed occurred in LMC motoneurons, in particular in peroneal motoneurons.

Misspecification of motoneuron pools

To assess how ectopic EVX2 interferes with MN specification, we compared group A and B deletions using the *Raldh2* and *Pea3* markers. The former labels the entire LMC (Sockanathan and Jessell 1998), and a comparison between Del(10–13), Del(10–13); $Evx2^{stop}$, and wild-type configurations revealed a posterior shift in the mutant patterns, coherent with the nerve root homeotic transformations. In addition, a marked decrease in signal intensity was scored in the Del(10–13) specimen, that is, when a genuine EVX2 protein was ectopically expressed. This effect was general, yet particularly obvious at dorsal root ganglia (DRG) level 21–22 (Fig. 9A).

At hindlimb level, *Pea3* is expressed by subsets of motoneuron pools within the LMC (Arber et al. 2000). In situ hybridization revealed the lumbar motor pools, with

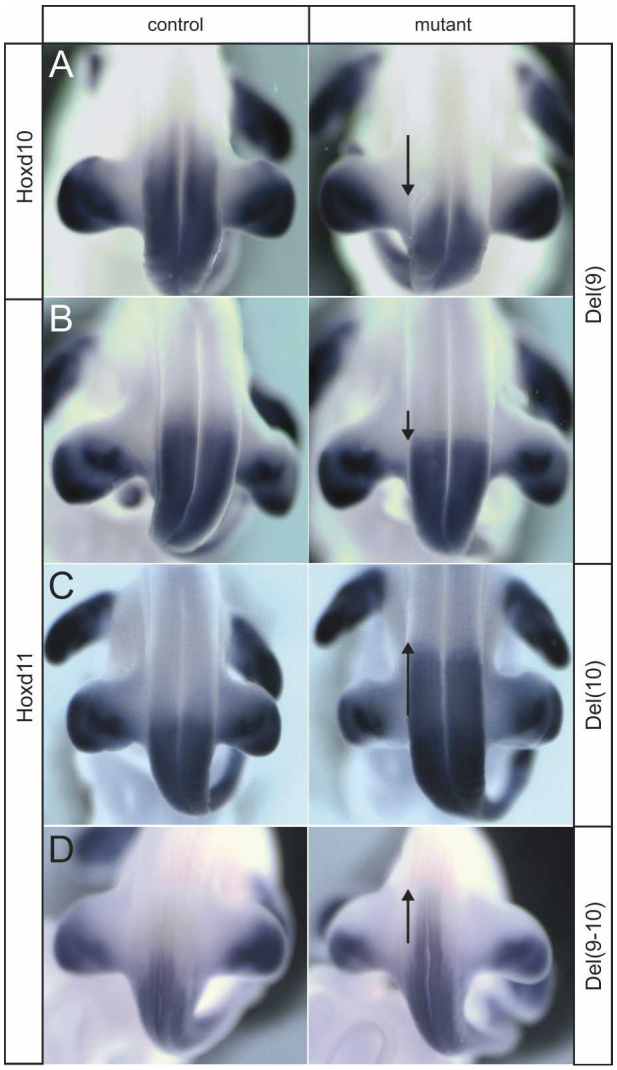

Figure 7. Spinal shifts in *Hox* gene expression in various deletion stocks. (*A*,*B*) The lumbar homeosis observed in the Del(9) allele (Fig. 5E) correlates with significant caudal shifts in the expression of both *Hoxd10* (*A*) and *Hoxd11* (*B*) genes. Consequently, while only *Hoxd9* is physically absent, the activities of *Hoxd10* and *Hoxd11* are also missing in the relevant lumbar region, leading to a severe anterior homeosis. (*C*) Conversely, a rostral shift of *Hoxd11* expression is scored in Del(10) animals, accounting for the unexpected posterior root transformation (Fig. 5B). (*D*) A comparable rostral shift of *Hoxd11* expression is seen in Del(9–10). In this case, however, the additional loss of *Hoxd9* function likely compensates for part of the *Hoxd11* gain of function, generating a new functional balance with a normal nerve root organization (Fig. 5C).

intermediate intensity in the 21st–22nd DRG region, a somewhat lower intensity in the 23rd–24th region, whereas a stronger signal was detected around the 25th level (Fig. 9B–E).

As for *Raldh2*, group B deletions showing nerve root homeotic transformations displayed rostro-caudal shifts of *Pea3*-positive cells. For example, embryos lacking the *HoxD* cluster, with a partial anterior homeosis, displayed a posterior shift of *Pea3*-positive MNs, most evident at the anterior lumbar level [Fig. 9B, Del(1–13)]. Conversely, posterior homeosis induced by the *Hoxd11* lumbar gain of function in Del(10) was accompanied by an anterior shift of the caudal *Pea3* pools [Fig. 9C, Del(10)]. In all cases, the extent of homeosis and motor pool shifts was coordinated and involved a maximum of one segment. Deletions without associated root homeosis [e.g., Del(8–10)] showed normal *Pea3* patterns (data not shown). Nerve roots homeosis thus reflected the shifts of motor pools induced by modified *Hoxd* gene expression as suggested by the *Lim1taulacZ* experiments.

Group A deletions showed a substantial loss of *Pea3*-positive cells at DRG levels 21–24, whereas the strong signal normally seen at the 25th level was shifted caudally in homozygous specimens [e.g., Del(10–13)] (Fig. 9D), the loss being already scored in *Irn* heterozygous animals (Fig. 9E). Because the latter animals otherwise maintained a normal nerve root pattern, we concluded that loss of *Pea3* signal is caused by the *Evx2* gain of function, rather than by alterations in *Hoxd* gene expression.

To further assess the fate of the LMC in our group A mutants, we immunostained neighbor sections of E14.5 Del(10–13) mutant animals with antibodies against HB9, whose robust expression labels the lateral subset of the LMC (LMCl) (Arber et al. 2000) and Islet1 (*Isl1*), a marker of the medial subset of the LMC (LMCm) as well as of the MMC (Tsuchida et al. 1994). A third set of sections was stained for cleaved *caspase-3*, to detect potential variation in the number of apoptotic cells (Wang et al. 2001). At DRG levels 21–22, where *Raldh2* and *Pea3* expression was mostly decreased in this mutant stock, a virtually complete disappearance of the lateral-most *Hb9* staining was observed, suggesting either the depletion or misidentification of the LMCl at this level (Supplementary Fig. S1A–C). However, apoptotic cells were not increased in number between E11.5 and E15.5 (Supplementary Fig. S1D–F). Since *Evx2*, as *Evx1*, is a post-mitotic marker for V0 interneurons, and because *Hb9* inactivation leads to an increased number of *Chx10*-positive V2 interneurons, we assessed potential MN respecification by looking at *Evx1* and *Chx10* (Arber et al. 1999; Thaler et al. 1999; Moran-Rivard et al. 2001). No abnormal expression of these markers was detected between E10.5 and E11.5 in group A mutants (data not shown).

Discussion

The mouse Irn *mutation is allelic to* HoxD

In the spinal cord, loss of function of *Hox* genes has been associated with motor alterations at the level of both brachial and lumbo-sacral plexii, leading to detectable handicaps (Carpenter et al. 1997; Tiret et al. 1998). In these cases, abnormal innervation of the limbs was accounted for by a misidentification of the related motoneurons, perhaps resulting from spinal cord homeosis.

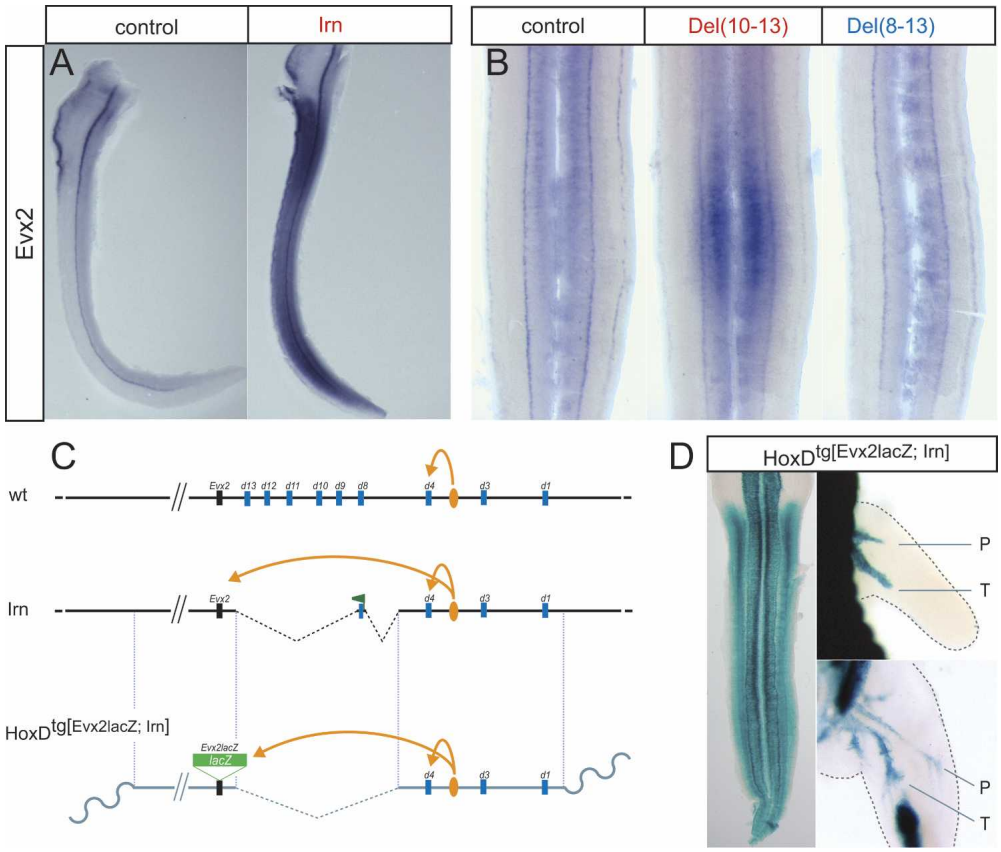

Figure 8. Complete leg paralysis in group A animals is associated with the gain of expression of *Evx2* in lumbar LMC motoneurons. (*A*) E11.5 half-spinal cords of control (*left*) and *Irn* mutants (*right*). (*Left*) Expression of *Evx2* is found in a column of interneurons. (*Right*) In the mutant stock, *Evx2* is largely gained in a broad *Hox*-like spinal domain. (*B*) E12.5 LS spinal cords in an open-book configuration. All group A animals displayed a related *Evx2* gain of expression, though limited to the ventral spinal cord at lumbar level [here Del(10–13)]. In contrast, less severely paralyzed (group B) animals sharing the same deletion breakpoint near *Evx2* are devoid of ectopic *Evx2* transcripts [e.g., Del(8–13)]. (*C*) In group A deletions, the *Evx2* gene responds to neural regulatory sequences normally acting on *Hoxd* genes (yellow arrows). A modified *HoxD* BAC clone, with a deletion mimicking *Irn* outer breakpoints and a *LacZ* reporter cassette within *Evx2* is used to generate transgenic mice ($HoxD^{tg[Evx2lacZ;Irn]}$). (*D*, *left* panel) X-gal staining of transgenic embryos confirms the impact of the deletion on *Evx2* regulation (open-book view). Axon fibers innervating the hindlimb, but not the forelimb, are labeled, demonstrating that the spinal gain of expression includes lumbar LMC motoneurons (*upper right* and *lower right* panels, E11.5 and E13.5 hindlimbs, respectively). (T) Tibial nerve; (P) peroneal nerve.

Our characterization of both the mouse *Ironside* mutation and of several engineered deletions in the *HoxD* cluster shed some light on the molecular etiology(ies) of *Hox*-induced motor defects, which cannot be solely explained in terms of homeotic transformations.

Irn mutant mice were isolated due to a severe hindlimb paralysis affecting heterozygous animals. The fact that animals heterozygous for a complete *HoxD* deletion do not display such a locomotion problem (Zakany et al. 2001) raised questions about the molecular nature of this mutation. The characterization of *Irn* confirmed that the *HoxD* cluster had been modified, yet it did not solve the abovementioned paradox, which was reinforced by subsequent analysis of several engineered *HoxD* deletions also revealing paralyses more severe than those associated with a mere cluster deletion. This latter observation ruled out the presence, in *Irn* mice, of additional *HoxD*-independent genetic modifications adding to the phenotype. Likewise, potential implications of either the first exon of *Hoxd8* or the 200-bp foreign fragment were ignored, as similar effects were obtained without such peculiarities. The *Irn* mutation was thus functionally considered as a simple large deletion removing from upstream of *Hoxd4* to upstream of *Hoxd13*.

Multiple factors induce distinct paralyses

The analysis of both the *Irn* mutation and our deleted stocks revealed multifactorial causes for the various paralyses, involving at least three aspects. First, all affected strains lacked *Hoxd10*, making *Hoxd10* inactivation mandatory for paralysis to occur. Second, a variety of either complete or incomplete nerve roots homeotic transformations was associated with the deleted configurations, which could impact on the organization of the lumbo-sacral plexus, leading to motor problems. Third, the strong paralysis observed in group A animals also involved a gain-of-function effect associated with the po-

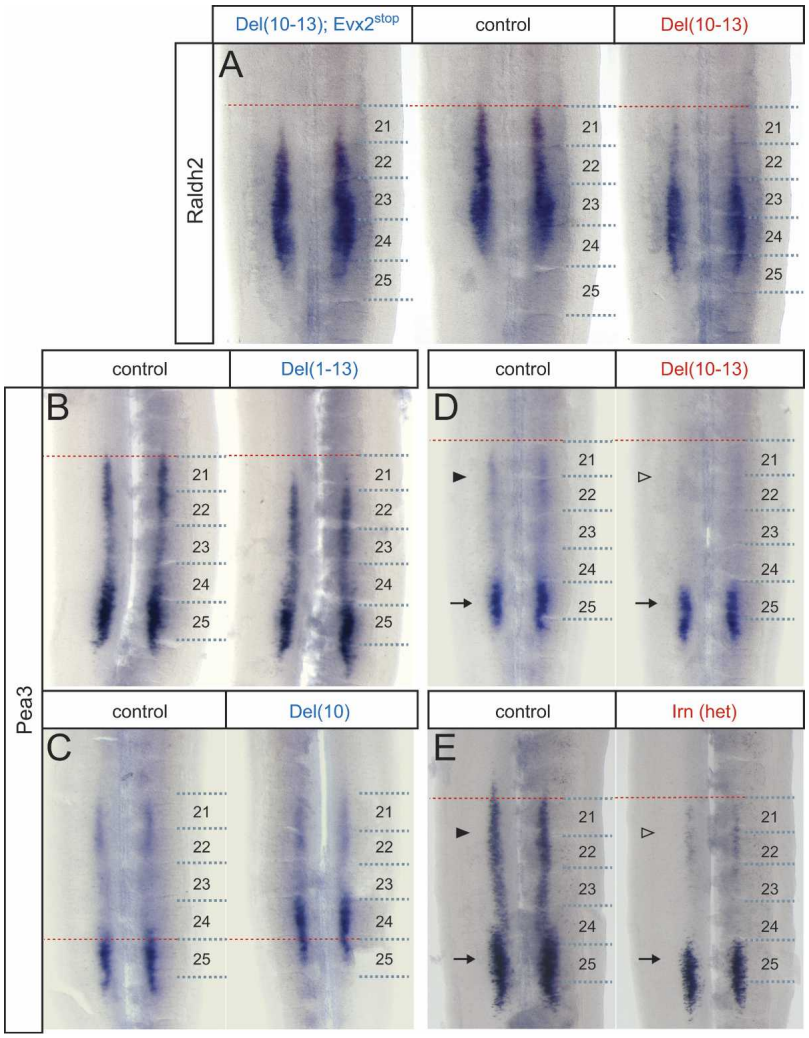

Figure 9. Dominant paralysis in group A specimens is associated with a massive loss of hindlimb LMC motoneurons, including *Pea3*-positive motor pools. (*A–E*) E12.0–E13.0 LS spinal cords in an open-book configuration. Numbers refer to DRG levels. (*A*) At lumbar level, the LMC position is revealed by *Raldh2* staining and appeared caudally shifted in both Del(10–13); $Evx2^{stop}$ and Del(10–13) alleles. However, only the latter group A allele is accompanied by a significant loss of signal at levels 21–22, suggesting a loss of MN innervating the hindlimb. (*B*,*C*) Group B alleles show *Pea3* expression reminiscent of the nerve root homeotic transformations scored after neurofilament stainings, with some motor pools shifted either caudally in anterior root transformations [Del(1–13)] (*B*) or rostrally in posterior transformations [Del(10)] (*C*). (*D*,*E*) More dramatic alterations of the *Pea3* expression domains are scored in group A mutants. Staining in the 21–24 region (arrowhead) is reduced in Del(10–13) homozygous, indicating that the corresponding motor pools are strongly depleted. A decrease in staining intensity is already visible in *Irn* heterozygotes in *E*. The *Pea3*-positive pools at level 25 appear normal (arrow), although slightly shifted caudally in Del(10–13) homozygous. Differences in staining intensities reflect differences in age, with E12.0 samples [Del(1–13), *Irn*] showing a stronger signal than E12.5–E13.0 samples [Del(10), Del(10–13)].

sition of the L1 breakpoint, since all group A deletions shared this 5′-extremity upstream of *Hoxd13*.

The loss of the embryonic peroneal nerve was occasionally observed in *Hoxd10* mutant hindlimbs, yet most adults showed a normal leg innervation (Carpenter et al. 1997). In our hands, these latter fetuses displayed peroneal defects classified as "thinner/shorter." In contrast, a proportion of E12.5 group B animals were of the "truncated" category, generally leading to adults lacking this particular nerve. Altogether, our group B animals were thus more severely affected than the *Hoxd10* mutant mice, which may result from the absence and/or deregulation of other *Hoxd* genes expressed at lumbosacral levels, an additive effect previously described for *Hoxd10* and *Hoxa10* (Wahba et al. 2001). However, the loss of the other *Hoxd* function has no effect as long as *Hoxd10* was present, and *Hoxa10* expression was found to be normal in group A embryos (data not shown). This and the fact that our group A animals are more affected than double group 10 mutants (Wahba et al. 2001) further suggest that additional alterations in gene activity are involved in the increased severity scored in group A animals.

While the extent of paralysis and the peroneal defects correlate well in the various alleles, other deficiencies participate in gait abnormality. Group B internal deletions, like *Hoxd10* inactivation (Carpenter et al. 1997), led to outer foot rotation, and additional innervation defects occurred beside the reduction of the peroneal branch such as a dorso-lumbar plexus deprived of fibers in group A deletions.

Nerve roots homeosis in HoxD *deletions*

The position of both embryonic nerve roots and adult LMC in *Hoxd10* mutants led Carpenter et al. (1997) to propose that alterations in MN positional identity are reflected by changes in peripheral innervation patterns; the 23rd nerve acquires a more anterior 22nd identity and ectopically projects to the lumbar plexus, thus reducing the number of axons projecting through the sacral plexus. In our hands, nerve root homeosis in $Hoxd10^{-/-}$ animals was most prominent as partial anterior transformations affecting the 25th–27th nerves, even though we consistently noticed a slight reduction of the 23rd nerve contribution to the lumbar plexus. Yet the analysis of

nerve roots in our mutants did not establish a firm correspondence between the type and/or level of homeotic transformations and the severity of the phenotype. For example, while reduced 23rd nerve contribution to the sacral plexus may lead to peroneal depletion, stronger peroneal phenotypes (and concomitant locomotion defects) were observed in the absence of homeosis, in some group B animals [e.g., Del(8–10)].

Conversely, homeotic transformations were scored in strains barely paralyzed, if at all [e.g., Del(9)]. In this case, it is unlikely that transformed 24th and 25th nerves could compensate for the redirection of some 23rd nerve fibers to the lumbar plexus, since the 24th root was systematically the most reluctant to anterior transformations. Altogether, nerve root homeosis was thus neither necessary, nor sufficient, for the emergence of a severely truncated peroneal branch. However, it could be instrumental in the occurrence of milder peroneal reductions, as for Del(9) embryos occasionally showing a thinner/shorter peroneal nerve.

Nerve root homeosis at lumbar levels was nevertheless always found in group A animals with complete paralysis, even though it was also observed for all deletions lacking *Hoxd10* and starting with the L1 breakpoint (including both A and B representatives). The *Lim1taulacZ* experiment suggests an explanation for this, as only group A alleles showed a robust and global lumbar *motor* homeosis. Therefore, anterior motor homeosis affecting the 23rd and 24th motor nerves might be critical for the loss of the dorso-sacral plexus and its emerging peroneal branch, whereas formation of this plexus is compatible with the converse posterior homeosis. We do not think that incorrect register between the limbs and the position of motoneurons participates in the phenotype, as the pelvic bone was found displaced accordingly. Also, complete anterior homeosis was described for *Hoxa10*$^{-/-}$ adult mice, without any paralysis (Rijli et al. 1995), further documenting that full anterior homeosis is compatible with normal motor innervation and suggesting that peripheral innervation defects derive from partial, rather than complete transformations in nerve identities.

Our conditional deletion approach makes it unlikely that loss of the *Hoxd* gene in limb mesenchyme is involved in the paralysis. Instead, shifts in the position of lumbar LMC, revealed either by the *Lim1taulacZ* reporter or by the rostro-caudal location of *Raldh2*- and *Pea3*-positive cells, are likely critical in nerve roots homeosis. The primary cause of paralysis thus lies in the misidentification, wrong position, or disappearance of pools of motoneurons, consequent to modifications in the structure of the *HoxD* cluster, which in turn lead to various *Hox* losses and/or gains of function derived from the reallocation of enhancer activity. The analysis of gene expression in our various deletions confirmed this hypothesis.

Ectopic expression of Evx2

In group A animals, *Evx2* adopted a *Hox* pattern up to various spinal cord rostral levels. Since all group A deletions share the same 5′-breakpoint, it is likely that the proximity of this breakpoint to the *Evx2* promoter triggers this up-regulation. Interestingly, some deletions carrying the same breakpoint showed a less severe paralysis (group B). However, such deletions were either associated with the inactivation of *Evx2* [Del(10–13); *Evx2*^{stop}] or showed normal *Evx2* expression [Del(8–13)]. In the latter case, the presence of a boundary or insulator element in the intergenic region "i" likely prevented *Evx2* misregulation, since further deletion of this region [in *Irn* or Del(i–13)] led to *Evx2* up-regulation and consequent severe paralysis. Finally, the transgene replacing the *HoxD* cluster in Del(1–13) animals is silent in the spinal cord (Spitz et al. 2001), indicating the concomitant deletion of neural enhancers in this group B allele, hence the failure to activate *Evx2*. *Evx2* was never found deregulated in deletions internal to the *HoxD* cluster.

Our transgenic approach, whereby the *Irn* deletion was reproduced and generated a similar gain of *Evx2* in the spinal cord, confirmed a role for the *Hoxd4–Hoxd3* neural enhancers (Morrison et al. 1997; Zhang et al. 1997) in ectopic *Evx2* expression. In these transgenic animals, the staining of hindlimb nerves by the *Evx2lacZ* reporter gene demonstrates misexpression within LMC neurons, supporting a detrimental function of EVX2 there. Likewise, the brachial nerves were not labeled in transgenic embryos, correlating with normal forelimb motility in *Irn* mutants.

Lumbo-sacral motoneuron alterations

The decrease in *Raldh2* and *Pea3* expression in our group A mutants indicated that some MN within the LMC were affected following ectopic expression of *Evx2*. The EVX2 protein labels V0 commissural interneurons (Moran-Rivard et al. 2001), which also express the paralogous gene *Evx1* (Dollé et al. 1994). While the function of *Evx2* in these cells is still elusive, *Evx1* mutant mice display cell fate transformations consistent with a role as a determinant of IN identity (Moran-Rivard et al. 2001). Furthermore, the *Evx1/2 Caenorhabditis elegans* gene *vab-7* (Esmaeili et al. 2002), while necessary for the determination of some motoneurons, can repress alternative MN fates, much in the same way as the *Drosophila* orthologous gene *evenskipped* (*eve*) (Landgraf et al. 1999; Broihier and Skeath 2002; Esmaeili et al. 2002; Odden et al. 2002). In both cases, pairs of homeodomain transcription factors specify differences between distinct MN identities through the inhibition of alternative fates, a mechanism also described in the specification of progenitor domains in the vertebrate neural tube (Jessell 2000).

In vertebrates, the MN-specific homeodomain factor *Hb9* can suppress interneuron specification (Arber et al. 1999; Thaler et al. 1999), suggesting that the converse influence may also occur. The quasidisappearance of strong *Hb9*-positive cells in the LMCl of group A mutants suggests that the antagonism between *eve* and *Hb9*, documented in *Drosophila*, is retained in vertebrates such that ectopic EVX product interferes with the

identification and/or fate of LMCl neurons. In this respect, it is noteworthy that the mouse EVX1 product can rescue *eve* mutant phenotype in the *Drosophila* nervous system, where abnormal MN specification coincides with the derepression of *Hb9* (Fujioka et al. 2003). Whether the loss of *Hb9* signal reflects an absence of LMCl is as yet unclear. At anterior LMC levels, the detection of the *Lim1* signal (specific for LMCl) on emerging axons suggests that at least some LMCl MNs are present, whereas the absence of dorso-sacral plexus at more posterior levels suggests the opposite.

Misspecification of motoneuron pools

While the fate of group A LMCl cells normally expressing *Hb9* is unknown, they likely do not enter apoptosis, as the overall number of apoptotic cells in this region was not significantly changed. Also, a shift of LMCl cells toward a V0 or V2 interneuron identity is unlikely, when considering the normal *Evx1* and *Chx10* expression in mutant spinal cord.

Pea3-positive lumbar pools do not contain MN innervating the distal limb compartment, either via the tibial or the peroneal nerves. Instead, they correspond to MN innervating more proximal limb targets (McHanwell and Biscoe 1981; Arber et al. 2000). The absence of *Pea3* signal observed in group A animals thus points to an innervation deficit in proximal hindlimb. This may explain the full leg paralysis observed in these specimens, as opposed to the distally restricted clubfoot phenotype of group B representatives, as the mere loss of the peroneal nerve is not expected to produce complete leg paralysis. Accordingly, in *EphA4* mutant mice, the lack of peroneal nerves due to the redirection of LMC projection toward the ventral limb mesenchyme leads to a limited clubfoot phenotype (Helmbacher et al. 2000). While this hypothesis explains the increased severity of group A deletions through an additive effect, its demonstration is made difficult by the absence of markers expressed in peroneal motor pools, which should then be defective in both group A and B mutants. Interestingly, more MN express *Pea3* at brachial versus lumbar levels, and a subtle defect in forelimb motor coordination was reported following *Pea3* inactivation (Livet et al. 2002).

We conclude that the two categories of paralyzed phenotypes reported here are likely produced by at least two different molecular mechanisms. The first one relies on the loss of *Hoxd10* function, which impacts mildly on the peroneal nerve branch, leading to a distal limb phenotype in both group A and B animals. The second factor is a gain of function of *Evx2*, which alters the determination of MN pools specific for more proximal innervation, thus leading to a full leg paralysis in group A animals only. The potential causal role of homeotic transformations in these phenotypes is more difficult to assess, as no strict correlation was observed between homeosis and the phenotypes. However, severely affected animals all had partial, rather than complete, transformations in their nerve roots patterns, indicating that an internal pattern disorganization is more detrimental than a complete shift.

Materials and methods

Isolation and mapping of the Ironside *(*Irn*) spontaneous mutation*

The *Irn* mutation was identified at The Jackson Laboratory, Maine, USA, from a single mutational event in an NZBW F1 mouse specimen showing severe hindlimb defects. In a cross with CAST/EiJ and C3HeB/FeJ strains, the region containing the mutation was narrowed to a 6-cM interval between markers *D2Mit10* and *D2Mit418* on mouse chromosome 2. As this mutation first appeared in F1 hybrid mice, polymorphic markers were used to establish that the mutation originated from the NZW/LacJ male parental chromosome and not the female NZB/B1NJ parental chromosome. The strain is currently maintained at The Jackson Laboratory on a B6C3Fe hybrid background. Breeding heterozygous animals generated mice with more severe hindlimb paralysis as well as digit defects. Southern blot and PCR analysis revealed that the mutation consisted in a complex deletion/insertion event in the *HoxD* cluster and allowed to further clone and sequence the breakpoints.

LoxP *mouse strains and targeted meiotic recombination (TAMERE)*

Two distinct parental strains carrying a *LoxP* site at the L1 position (Fig. 2) were used to produce genomic rearrangements in vivo. One strain contained a mutation within the *Evx2* gene (Hérault et al. 1996) and was used to produce the Del(10–13); $Evx2^{stop}$ allele. All other deletions with a L1 breakpoint were obtained via another *LoxP* strain associated to a short deletion removing a conserved intergenic region upstream of *Evx2* (Kmita et al. 2002). For the sake of clarity, and because this intergenic sequence did not interfere either with the phenotypes or with the regulatory effects reported here, it is not mentioned in Figure 2. The L4 strain was already described (Gérard et al. 1996). The L5, L6, L7, and L8 strains were produced by routine ES cell technology, and carry a single *LoxP* site at the following positions: between *Hoxd10* and *Hoxd9* (L5: AAGGAGA TGGGAGGA*CTGGAGAAGACCTAG), between *Hoxd9* and *Hoxd8* (L6: TTTCCGGACAGGCGC*TCGAGATGTAGCAAA), 3′ to *Hoxd8* (L7: GCACTTACGTGCATG*CTGCCAAAACA TTTG), and 5′ to *Hoxd4* (L8: GACAGCTCTCCTCTA*AGCT TCTCTACCAAC). The various crosses to obtain targeted meiotic recombination events from two distinct *LoxP* parental strains, in the presence of the *Sycp1-Cre* transgene, are like those described elsewhere (Hérault et al. 1998). Animals heterozygous for a given deletion event were recovered with a frequency of 0.1%–5%.

The Flox(4–13) chromosome was produced by two rounds of targeting in ES cells as already described for the corresponding deletion (Zakany and Duboule 1999); the line used here corresponds to the germline transmission of the floxed clone before Cre treatment in vitro. The L11 position corresponds to a *LoxP* targeting event used to produce a deletion of the entire *HoxD* cluster in ES cells (Zakany et al. 2001). The *Lim1taulacZ* mouse strain was provided by A. Kania and T. Jessell (Howard Hughes Medical Institute, Columbia University, New York), and the *Hoxd10* insertional mutant stock by E. Carpenter (University of California at Los Angeles School of Medicine, Los Angeles, CA).

HoxD *BAC recombination and transgenesis*

A mouse BAC (RPCI23-400H17) carrying the entire *HoxD* complex and ~100 kb of centromeric sequence (Spitz et al. 2001) was

used to generate a large deletion removing the *Hoxd13* to *Hoxd8* genes. A kanamycine resistance gene was amplified by PCR using primers bearing ~50-pb homology to the genomic sequences located on each side of the intended deletion at their 5′ extremities (5′ deletion/*Kan*^{R}: CGCGACACCTTCATTCATT AGTGGTTTTGAAACTACCTTGCACCTTTTAAGTAACAT CGGATCCTAGTAAGCCACG; 3′ deletion/*Kan*^{R}: CCACCCA AGAAGAAACCAAGGCCAGGACATTGGCTCCCCAGTTC TATAAATAGAAGTCCCCTACCCGGTAGAATTC). Sequence homology was selected such that the engineered breakpoints on the BAC exactly matched the outer breakpoints mapped in the *Irn* mutant. Upon bacterial electroporation, the resulting PCR product thus replaced 50 kb of 400H17 BAC sequence (including the *Hoxd13* to *Hoxd8* genes) by the *Kan*^{R} selection cassette. To monitor *Evx2* gene expression from the deleted 400H17 BAC, the *LacZ* coding sequence was inserted in frame such as to disrupt the homeodomain located in the second exon. Primers bearing convenient restriction sites and 50-pb homology to the *Evx2* homeodomain at their 5′ extremities were used to amplify a plasmid backbone containing the R6K origin of replication (*BamHI/3′homeo/R6K*: GGCGGATCCTACAGGGAGAACTA CGTGTCTCGGCCCCGCCGGTGCGAGCTGGCCGCTGCA CTCACCCCTCTTTAATACGACGGGC; *SalI/5′homeo/KpnI/ R6K*: ATCGTCGACCGAACTCTTTCTCCAGGCGCGCGAT CTGTTCGCGGGTGAATGCCGTACGGTATCGCGGTACC CTGTGAATGCGCAAAC). Following the conventional cloning of a *LacZ-zeocin*^{R} cassette in this customized plasmid backbone, the insert carrying the *LacZ-zeocin*^{R} flanked by the two homology arms was excised and electroporated into bacterial cells containing the deleted 400H17 BAC. After linearization, the modified BAC was introduced in C57BL/6XDBA F1 fertilized mouse eggs by pronuclear injection.

Whole-mount in situ hybridization (WISH), immunochemistry, and X-gal stainings

WISH was carried out on fetuses between 11.5 and 12.5 d, using standard procedures and previously described probes. In several cases, the spinal cord was opened before hybridization for better probe accessibility. After staining, entire or half-spinal cords were dissected out and mounted in PBS/glycerol under a coverslip. Entire spinal cords are presented in an open-book configuration, viewed from a ventral aspect (Livet et al. 2002). Whole-mount neurofilament immunostainings were carried out on fetuses between 11.5 and 13.5 d, using standard procedures. The antibodies were anti-NF160 (clone NN18, Sigma N-5264) and anti-mouse Ig Fab HRP conjugate (Sigma A-3882). After antibody incubation, the embryos were stained with DAB substrate and cleared by dehydration in methanol, followed by incubation in BABB (1:2 benzyl alcohol/benzyl benzoate). Following X-gal detection of *LacZ* activity in BAC transgenic and *Lim1taulacZ* experiments, the embryos were cleared by the same procedure.

Immunohistochemistry

The antibodies used were rabbit anti-*Isl1* (A8; A. Pierani [Ecole Normale Superieure, Paris, France] and T. Jessell), rabbit anti-*Hb9* (S. Arber [Biozentrum, University of Basel, Basel, Switzerland]), and rabbit anti-cleaved caspase-3 (Asp 175) for detection of apoptotic cells (Cell Signaling Technology).

Leg footprints

Adult mice were encouraged to run on a light-sensitive film after having their hindfeet soaked in developer solution. After processing, exposed regions correspond to footprints.

Acknowledgments

We thank S. Arber, T. Jessel, and A. Pierani for probes and antibodies; A. Kania, T. Jessell, E. Carpenter, M. Logan, M. Kmita, and J. Zakany for mice; and S. Arber and J. Zakany for discussions and suggestions. This work was supported by funds from the canton de Genève, the Claraz and Louis Jeantet Foundations, the Swiss National Research Fund, the National Research Centre (NCCR) "Frontiers in Genetics," and the EU programmes "EUMORPHIA" and "Cells into Organs."

References

Arber, S., Han, B., Mendelsohn, M., Smith, M., Jessell, T.M., and Sockanathan, S. 1999. Requirement for the homeobox gene Hb9 in the consolidation of motor neuron identity. *Neuron* **23:** 659–674.

Arber, S., Ladle, D.R., Lin, J.H., Frank, E., and Jessell, T.M. 2000. ETS gene Er81 controls the formation of functional connections between group Ia sensory afferents and motor neurons. *Cell* **101:** 485–498.

Broihier, H.T. and Skeath, J.B. 2002. *Drosophila* homeodomain protein dHb9 directs neuronal fate via crossrepressive and cell-nonautonomous mechanisms. *Neuron* **35:** 39–50.

Carpenter, E.M. 2002. Hox genes and spinal cord development. *Dev. Neurosci.* **24:** 24–34.

Carpenter, E.M., Goddard, J.M., Davis, A.P., Nguyen, T.P., and Capecchi, M.R. 1997. Targeted disruption of Hoxd-10 affects mouse hindlimb development. *Development* **124:** 4505–4514.

Dasen, J.S., Liu, J.P., and Jessell, T.M. 2003. Motor neuron columnar fate imposed by sequential phases of Hox-c activity. *Nature* **425:** 926–933.

Davenne, M., Maconochie, M.K., Neun, R., Pattyn, A., Chambon, P., Krumlauf, R., and Rijli, F.M. 1999. Hoxa2 and Hoxb2 control dorsoventral patterns of neuronal development in the rostral hindbrain. *Neuron* **22:** 677–691.

Dollé, P., Izpisua-Belmonte, J.C., Brown, J.M., Tickle, C., and Duboule, D. 1991. HOX-4 genes and the morphogenesis of mammalian genitalia. *Genes & Dev.* **5:** 1767–1776.

Dollé, P., Dierich, A., LeMeur, M., Schimmang, T., Schuhbaur, B., Chambon, P., and Duboule, D. 1993. Disruption of the Hoxd-13 gene induces localized heterochrony leading to mice with neotenic limbs. *Cell* **75:** 431–441.

Dollé, P., Fraulob, V., and Duboule, D. 1994. Developmental expression of the mouse Evx-2 gene: Relationship with the evolution of the HOM/Hox complex. *Development* **Suppl:** 143–153.

Duboule, D. and Morata, G. 1994. Colinearity and functional hierarchy among genes of the homeotic complexes. *Trends Genet.* **10:** 358–364.

Esmaeili, B., Ross, J.M., Neades, C., Miller III, D.M., and Ahringer, J. 2002. The *C. elegans* even-skipped homologue, vab-7, specifies DB motoneurone identity and axon trajectory. *Development* **129:** 853–862.

Fujioka, M., Lear, B.C., Landgraf, M., Yusibova, G.L., Zhou, J., Riley, K.M., Patel, N.H., and Jaynes, J.B. 2003. Even-skipped, acting as a repressor, regulates axonal projections in *Drosophila*. *Development* **130:** 5385–5400.

Gaunt, S.J., Sharpe, P.T., and Duboule, D. 1988. Spatially restricted domains of homeogene transcripts in mouse embryos: Relation to a segmented body plan. *Development* **Supp. 104:** 169–180.

Gérard, M., Chen, J.Y., Gronemeyer, H., Chambon, P., Duboule, D., and Zakany, J. 1996. In vivo targeted mutagenesis of a regulatory element required for positioning the Hoxd-11 and

Hoxd-10 expression boundaries. *Genes & Dev.* **10:** 2326–2334.
Graham, A., Maden, M., and Krumlauf, R. 1991. The murine Hox-2 genes display dynamic dorsoventral patterns of expression during central nervous system development. *Development* **112:** 255–264.
Helmbacher, F., Schneider-Maunoury, S., Topilko, P., Tiret, L., and Charnay, P. 2000. Targeting of the EphA4 tyrosine kinase receptor affects dorsal/ventral pathfinding of limb motor axons. *Development* **127:** 3313–3324.
Hérault, Y., Hraba-Renevey, S., van der Hoeven, F., and Duboule, D. 1996. Function of the Evx-2 gene in the morphogenesis of vertebrate limbs. *EMBO J.* **15:** 6727–6738.
Hérault, Y., Rassoulzadegan, M., Cuzin, F., and Duboule, D. 1998. Engineering chromosomes in mice through targeted meiotic recombination (TAMERE). *Nat. Genet.* **20:** 381–384.
Jessell, T.M. 2000. Neuronal specification in the spinal cord: Inductive signals and transcriptional codes. *Nat. Rev. Genet.* **1:** 20–29.
Kania, A., Johnson, R.L., and Jessell, T.M. 2000. Coordinate roles for LIM homeobox genes in directing the dorsoventral trajectory of motor axons in the vertebrate limb. *Cell* **102:** 161–173.
Kmita, M. and Duboule, D. 2003. Organizing axes in time and space; 25 years of colinear tinkering. *Science* **301:** 331–333.
Kmita, M., Tarchini, B., Duboule, D., and Herault, Y. 2002. Evolutionary conserved sequences are required for the insulation of the vertebrate Hoxd complex in neural cells. *Development* **129:** 5521–5528.
Landgraf, M., Roy, S., Prokop, A., VijayRaghavan, K., and Bate, M. 1999. even-skipped determines the dorsal growth of motor axons in *Drosophila*. *Neuron* **22:** 43–52.
Livet, J., Sigrist, M., Stroebel, S., De Paola, V., Price, S.R., Henderson, C.E., Jessell, T.M., and Arber, S. 2002. ETS gene Pea3 controls the central position and terminal arborization of specific motor neuron pools. *Neuron* **35:** 877–892.
Logan, M., Martin, J.F., Nagy, A., Lobe, C., Olson, E.N., and Tabin, C.J. 2002. Expression of Cre Recombinase in the developing mouse limb bud driven by a Prxl enhancer. *Genesis* **33:** 77–80.
Lumsden, A. and Krumlauf, R. 1996. Patterning the vertebrate neuraxis. *Science* **274:** 1109–1115.
McGinnis, W. and Krumlauf, R. 1992. Homeobox genes and axial patterning. *Cell* **68:** 283–302.
McHanwell, S. and Biscoe, T.J. 1981. The localization of motoneurons supplying the hindlimb muscles of the mouse. *Philos. Trans. R Soc. Lond. B Biol. Sci.* **293:** 477–508.
Moran-Rivard, L., Kagawa, T., Saueressig, H., Gross, M.K., Burrill, J., and Goulding, M. 2001. Evx1 is a postmitotic determinant of v0 interneuron identity in the spinal cord. *Neuron* **29:** 385–399.
Morrison, A., Ariza-McNaughton, L., Gould, A., Featherstone, M., and Krumlauf, R. 1997. HOXD4 and regulation of the group 4 paralog genes. *Development* **124:** 3135–3146.
Odden, J.P., Holbrook, S., and Doe, C.Q. 2002. *Drosophila* HB9 is expressed in a subset of motoneurons and interneurons, where it regulates gene expression and axon pathfinding. *J. Neurosci.* **22:** 9143–9149.
Rijli, F.M., Matyas, R., Pellegrini, M., Dierich, A., Gruss, P., Dolle, P., and Chambon, P. 1995. Cryptorchidism and homeotic transformations of spinal nerves and vertebrae in Hoxa-10 mutant mice. *Proc. Natl. Acad. Sci.* **92:** 8185–8189.
Shah, V., Drill, E., and Lance-Jones, C. 2004. Ectopic expression of Hoxd10 in thoracic spinal segments induces motoneurons with a lumbosacral molecular profile and axon projections to the limb. *Dev. Dyn.* **231:** 43–56.
Sockanathan, S. and Jessell, T.M. 1998. Motor neuron-derived retinoid signaling specifies the subtype identity of spinal motor neurons. *Cell* **94:** 503–514.
Spitz, F., Gonzalez, F., Peichel, C., Vogt, T.F., Duboule, D., and Zakany, J. 2001. Large scale transgenic and cluster deletion analysis of the HoxD complex separate an ancestral regulatory module from evolutionary innovations. *Genes & Dev.* **15:** 2209–2214.
Spitz, F., Gonzalez, F., and Duboule, D. 2003. A global control region defines a chromosomal regulatory landscape containing the HoxD cluster. *Cell* **113:** 405–417.
Thaler, J., Harrison, K., Sharma, K., Lettieri, K., Kehrl, J., and Pfaff, S.L. 1999. Active suppression of interneuron programs within developing motor neurons revealed by analysis of homeodomain factor HB9. *Neuron* **23:** 675–687.
Tiret, L., Le Mouellic, H., Maury, M., and Brulet, P. 1998. Increased apoptosis of motoneurons and altered somatotopic maps in the brachial spinal cord of Hoxc-8-deficient mice. *Development* **125:** 279–291.
Trainor, P.A. and Krumlauf, R. 2001. Hox genes, neural crest cells and branchial arch patterning. *Curr. Opin. Cell Biol.* **13:** 698–705.
Tsuchida, T., Ensini, M., Morton, S.B., Baldassare, M., Edlund, T., Jessell, T.M., and Pfaff, S.L. 1994. Topographic organization of embryonic motor neurons defined by expression of LIM homeobox genes. *Cell* **79:** 957–970.
Wahba, G.M., Hostikka, S.L., and Carpenter, E.M. 2001. The paralogous Hox genes Hoxa10 and Hoxd10 interact to pattern the mouse hindlimb peripheral nervous system and skeleton. *Dev. Biol.* **231:** 87–102.
Wang, J., Silva, J.P., Gustafsson, C.M., Rustin, P., and Larsson, N.G. 2001. Increased in vivo apoptosis in cells lacking mitochondrial DNA gene expression. *Proc. Natl. Acad. Sci.* **98:** 4038–4043.
Yokouchi, Y., Sakiyama, J., and Kuroiwa, A. 1995. Coordinated expression of Abd-B subfamily genes of the HoxA cluster in the developing digestive tract of chick embryo. *Dev. Biol.* **169:** 76–89.
Zakany, J. and Duboule, D. 1999. *Hoxd* genes and the making of sphincters. *Nature* **401:** 761–762.
Zakany, J., Kmita, M., Alarcon, P., de la Pompa, J., and Duboule, D. 2001. Localized and transient transcription of Hox genes suggests a link between patterning and the segmentation clock. *Cell* **106:** 207–217.
Zhang, F., Popperl, H., Morrison, A., Kovacs, E.N., Prideaux, V., Schwarz, L., Krumlauf, R., Rossant, J., and Featherstone, M.S. 1997. Elements both 5′ and 3′ to the murine Hoxd4 gene establish anterior borders of expression in mesoderm and neurectoderm. *Mech. Dev.* **67:** 49–58.

HoxD cluster scanning deletions identify multiple defects leading to paralysis in the mouse mutant *Ironside*

Basile Tarchini, Thi Hanh Nguyen Huynh, Greg A. Cox, et al.

Genes Dev. 2005, **19:**
Access the most recent version at doi:10.1101/gad.351105